

Magnetic Inversion to Recover Compact Structures by an Arctangent Stabilizer

Rudarsko-geološko-naftni zbornik
(The Mining-Geology-Petroleum Engineering Bulletin)
DOI: 10.17794/rgn.2026.1.3

Original scientific paper



Sahar Moazam¹✉, Mohammad Rezaie^{1*}✉

¹ Department of Mining Engineering, Faculty of Engineering, Malayer University, Malayer, Iran.

Abstract

This study introduces a novel method for the inversion of magnetic data using a focusing inversion technique. The method utilizes an arctangent stabilizing functional, which is reformulated into a pseudo-quadratic form by a weighting matrix. To optimize the process, the reweighted regularized conjugate gradient (RRCG) method is employed. The proposed technique is effective in restoring compact structures in subsurface structures without the need for a focusing parameter. The inversion method involves constructing an objective function for minimization, which incorporates the discrepancy between observed and predicted data and the deviation of the model from expected characteristics, which is known as the stabilizing functional. The data fit component determines how closely the inversion results match the observed measurements, while the model regularization term influences specific desired properties of the reconstructed density distribution. The study demonstrates the effectiveness of the proposed technique through its application to a synthetic dataset and one real-world aeromagnetic dataset from the McFaulds Lake area in Ontario, Canada.

Keywords:

magnetic; inversion; stabilizer; arctangent; McFaulds Lake

1. Introduction

In exploration programs, geophysicists analyze measured magnetic data to determine the distribution of subsurface physical properties, particularly magnetic susceptibility. This process, known as the inverse magnetic problem, involves constructing a model that fits the observed data. However, the problem is mathematically ill-posed, meaning it lacks a unique or stable solution. To mitigate the inherent non-uniqueness and instability, regularization techniques are essential (Fedi & Rapolla, 1999; Cuma et al., 2012). By applying these methods, geophysicists can develop more reliable subsurface models, which are critical for resource exploration and geological interpretation.

Over the years, numerous regularization techniques have been developed for potential field data inversion. Selecting an appropriate method depends on choosing a model criterion that incorporates the desired geological characteristics. Recent decades have seen significant advancements and diversification in this field (Li & Oldenburg, 1998; Portniaguine & Zhdanov, 1999, 2002; Lelièvre et al., 2009; Pilkington, 2009; Marchetti et al., 2014; Meng, 2018; Peng et al., 2018).

In the inversion of magnetic field data, regularization techniques based on minimum norm or maximum smoothness stabilizers are commonly used. These methods typically produce smooth susceptibility models. However, they may not be suitable for scenarios involving anomalous bodies with discrete, blocky structures.

To address this issue, researchers have developed non-smooth inversion techniques to reconstruct geologically realistic models with sharp, blocky features. These techniques often employ stabilizing functionals that enforce compactness. The foundational work in compact gravity inversion was introduced by Last and Kubik (1983), who minimized the spatial extent of the density distribution responsible for observed gravity anomalies. Portniaguine and Zhdanov (1999) extended this concept by applying it to the gradient of the physical property model, developing a focused inversion technique. However, both methods require careful selection of the focusing parameter.

Bertete-Aguirre et al. (2002) incorporated the total variation (TV) function as a stabilizing functional, imposing sparsity constraints on the model gradient – equivalent to applying an L1-norm to the gradient. Similarly, a Cauchy norm stabilizer has been proposed for sparsity constraints (Pilkington, 2009; Rezaie et al., 2017). Zhao et al. (2016) introduced a novel approach to focused inversion using a stabilizing functional based on the exponential variation of model parameters. While

* Corresponding author: Mohammad Rezaie
e-mail address: mohamad1rezaie@malayeru.ac.ir

Received: 22 April 2025. Accepted: 8 July 2025.

Available online: 2 January 2026

this method eliminates the need for a focusing parameter, it produces inverted models with an elongated tail at the base of the anomalous body. More recently, **Rezaie (2019)** applied a zero-order minimum entropy regularization term to effectively delineate sharp edges in reconstructed density models.

Geophysical inversion methods that employ focusing stabilizers require a parameter to control either the model's compactness or the sharpness of recovered geological boundaries. This parameter – commonly called the focusing or compactness parameter – varies depending on the specific model being used. Typically, its optimal value is determined through an iterative process involving multiple inversions and result-based adjustments. Such trial-and-error approaches remain standard practice for fine-tuning inversion processes (**Pilkington, 2009; Xiang et al., 2017; Rezaie, 2019, 2020**).

Recent developments have introduced parameter-free alternatives. **Rezaie (2023)** proposed a novel stabilization method using an error function that eliminates dependency on the focusing parameter. Similarly, **Hu et al. (2017)** developed an arctangent-based compactness constraint for ground-penetrating radar data inversion, enabling sharp boundary reconstruction without parameter tuning.

This study presents a novel focusing inversion technique for magnetic data that employs an arctangent stabilizing functional reformulated as a pseudo-quadratic function of model parameters through a weighting matrix, optimized using the reweighted regularized conjugate gradient (RRCG) method, and validated through successful applications to both synthetic and real-world field datasets.

2. Methods

2.1. Forward modelling

The magnetic data observed at Earth's surface are primarily caused by induced magnetization effects. Forward modelling aims to compute this magnetic field, which arises from the distribution of magnetic susceptibility (κ) in subsurface materials. The total magnetic field component (\bar{T}) at an observation point \mathbf{r}_0 outside the magnetic source region can be expressed as (**Blakeley, 1995**):

$$\bar{T}(\mathbf{r}_0) = -C \nabla \int_{\mathbf{R}} \mathbf{J}(\mathbf{r}) \cdot \nabla \frac{1}{|\mathbf{r}_0 - \mathbf{r}|} dV \quad (1)$$

where $C=1 \times 10^{-7}$ (H.m⁻¹), \mathbf{R} is the volume occupied by the causative body, \mathbf{r}_0 denotes the observation point, \mathbf{r} represents the position of a volume element dV of the source body and $\mathbf{J}=\mathbf{J}_i+\mathbf{J}_r$ is the total magnetization vector that is the sum of induced and remanent magnetizations. Often, we ignore the remanent component and the total magnetization vector can be obtained by the following formula:

$$\mathbf{J}_i = \kappa \mathbf{H} \quad (2)$$

where \mathbf{H} is the Earth's magnetic field and κ represents magnetic susceptibility. To compute the total magnetic field component in **Equation 1**, the subsurface beneath the survey area is discretized into a series of rectangular prismatic cells. Each prism has predefined dimensions and location, with an assigned uniform magnetic susceptibility value. The foundational method for calculating the magnetic response of such rectangular prisms was developed by **Bhattacharyya (1964)**, with later refinements by **Rao and Babu (1991)** improving computational efficiency for modern computer-based implementations. In this study, we compute the magnetic signature of individual prismatic bodies using the **Rao and Babu (1991)** formulation. **Blakely (1995)** further contributed a concise mathematical representation of surface magnetic field data, compactly expressing the relationship between subsurface magnetic properties and surface observations as follows:

$$\mathbf{d}_{N \times 1} = \mathbf{G}_{N \times M} \times \boldsymbol{\kappa}_{M \times 1} \quad (3)$$

where N represents the total number of measurement locations at the surface, and M denotes the number of rectangular prisms used to discretize the subsurface in the model. The vector $\boldsymbol{\kappa}$ contains the unknown model parameters, which in this context represent the magnetic susceptibilities of each subsurface prism. The vector \mathbf{d} comprises the measured magnetic field data from the survey, while matrix \mathbf{G} serves as the forward operator that describes how each subsurface prism contributes to the magnetic field at each observation point.

2.2. Inversion method

To perform quantitative magnetic data inversion, we construct an objective function comprising two key components: (1) a data misfit term measuring the discrepancy between observed and predicted data, and (2) a regularization term controlling model characteristics. The data misfit quantifies how well the inversion results match field measurements, while the regularization term constrains the solution to exhibit desired physical properties. Following standard practice in geophysical inversion, we employ Tikhonov regularization (**Tikhonov & Arsenin, 1977**) to ensure stable solutions:

$$\Phi(\boldsymbol{\kappa}) = \mathbf{W}_d (\mathbf{G}\boldsymbol{\kappa} - \mathbf{d})_2^2 + \lambda S(\boldsymbol{\kappa}) \quad (4)$$

where N is the regularization parameter. $S(\boldsymbol{\kappa})$ represents the stabilizing functional and the first term is weighted data misfit, \mathbf{W}_d represents the weighting matrix associated with the data:

$$\mathbf{W}_d = \text{diag} \left(\frac{1}{\sigma_1}, \dots, \frac{1}{\sigma_i} \right) \quad (5)$$

where σ_i represents the standard deviation of the i^{th} measurement. This study investigates a compactness

constraint based on an arctangent function, designed to improve the delineation of sharp boundaries between subsurface structures. The stabilizing functional can be expressed as:

$$S(\kappa) = \|W_e \kappa\|_2^2 \tag{6}$$

where W_e is a diagonal model weighting matrix which is dependent on model parameters and can be given by (Hu et al., 2017):

$$W_e = \text{diag} \left(\sqrt{\frac{\arctan \sqrt{\kappa^2 + \mu^2}}{\kappa^2 + \varepsilon^2}} \right) \tag{7}$$

where ε and μ are small, non-zero constants introduced to prevent mathematical singularities and ensure numerical stability. While these parameters serve this essential computational purpose, they have negligible impact on the model parameters themselves. The arctangent functional provides an efficient focusing inversion method for magnetic data that offers two key advantages: (1) it eliminates the need for a focusing parameter, significantly simplifying implementation, and (2) it maintains robust performance in recovering subsurface structures.

Li and Oldenburg (1998) demonstrated that magnetic data inherently possesses limited depth resolution due to the fundamental nature of potential field measurements. This characteristic makes precise depth determination of magnetic sources particularly challenging. To mitigate the natural tendency of susceptibility models to concentrate near the surface, we incorporate a depth weighting matrix defined as:

$$W_z = \text{diag} \left[\frac{1}{z^2} \right] \tag{8}$$

where z is the depth of the model parameter and η is set to 3 in magnetic inversion (Li & Oldenburg, 1998). Moreover, the algorithm must ensure that the model adheres to the specified upper and lower susceptibility limits until a satisfactory model is obtained (Portniaguine & Zhdanov, 1999, 2002).

$$\kappa = \begin{cases} b & \text{if } \kappa < b \\ a & \text{if } \kappa > a \end{cases} \tag{9}$$

where b and a represent the lower and upper bounds of magnetic susceptibility, respectively. We solve this magnetic focusing inversion problem through an iterative approach using the reweighted regularized conjugate gradient (RRCG) method (Zhdanov, 2015), implemented as follows:

$$r_n = W_d (G(\kappa_n) - d), s_n = W_{en} W_z (\kappa_n),$$

$$I_{(k_n)}^\lambda = I_{(k_n)}^{\lambda_n} = G^T W_d^2 r_n + \lambda_n W_{en} W_z s_n,$$

$$\beta_{n+1}^\lambda = \frac{\|I_{(k_{n+1})}^\lambda\|^2}{\|I_{(k_n)}^\lambda\|^2}, \tilde{I}_{(k_n)}^{\lambda_n} = I_{(k_n)}^{\lambda_n} + \beta_n^{\lambda_n} \tilde{I}_{(k_{n-1})}^{\lambda_{n-1}}, \tilde{I}_0^{\lambda_0} = I_0^{\lambda_0},$$

$$\omega_n^{\lambda_n} = \frac{\left(\tilde{I}_{(k_n)}^{\lambda_n^T} I_{(k_n)}^{\lambda_n} \right)}{\tilde{I}_{(k_n)}^{\lambda_n^T} \left(G^T W_d^2 G + \lambda W_{en}^2 W_k^2 \right) I_{(k_n)}^{\lambda_n}},$$

$$\kappa_{n+1} = \kappa_n - \kappa_n^{\lambda_n} \tilde{I}_{(k_n)}^{\lambda_n}, \gamma = \frac{\|s_{n+1}\|^2}{\|s_n\|^2},$$

$$\lambda_1 = \frac{\|W_d (G\kappa_1 - d)\|^2}{\|\kappa_1\|_2^2}$$

$$\lambda_{n+1} = \lambda_n, \text{ if } \gamma \leq 1, \text{ and } \lambda_{n+1} = \frac{\lambda_n}{\gamma}, \text{ if } \gamma > 1$$

$$\lambda'_{n+1} = q \lambda_{n+1}, q < 1, \text{ if } \|W_d r_n\|^2 - \|W_d r_{n+1}\|^2 < 0.01 \|W_d r_n\|^2,$$

$$\lambda'_{n+1} = q \lambda_{n+1}, q < 1, \text{ if } \|W_d r_n\|^2 - \|W_d r_{n+1}\|^2 < 0.01 \|W_d r_n\|^2 \tag{10}$$

The algorithm converges to the solution when the normalized misfit arrives at the given level δ_0 (Rezaie, 2019, 2020):

$$\frac{\|W_d (G\kappa_n - d)\|_2^2}{\|W_d d\|_2^2} \leq \delta_0 \tag{11}$$

The RRCG is an efficient iterative solver that does not require constructing large $M \times M$ matrices or computing their inverses, unlike methods such as Gauss-Newton, Levenberg-Marquardt, and other IRLS algorithms. Another advantage of the RRCG algorithm is its ability to automatically select the regularization parameter through an adaptive process during iterations. This avoids the need to solve the inverse problem multiple times in each iteration.

2.3. Synthetic model

To illustrate the application of our proposed method, we examine a synthetic data scenario featuring distinct anomalous structures. According to Equation 7, we need to select two parameters μ and ε , that we set both equal to 1×10^{-16} for all models in this paper.

The synthetic model consisted of four blocks with a susceptibility of 0.05 SI and the background susceptibility is uniform that is equals to zero. The total magnetic field anomaly was calculated at ground level, based on an inducing magnetic field which has the inclination of 65° and the declination of -25° . The inducing field strength is 50,000 nT. The model covers an area extending 90 m to the north and 90 m to the east. The subsurface was divided into 23328 equal-sized rectangular

Table 1. Size parameters of the buried prisms in the synthetic model

Block number	x × y × z dimensions (m)	Depth to top (m)
(1)	125 × 125 × 125	25
(2)	125 × 125 × 125	50
(3)	125 × 125 × 125	50
(4)	125 × 125 × 125	25

prisms for inversion. Each prism measured 12.5 m on each side, arranged in a $36 \times 36 \times 18$ grid. There are four buried blocks in the area that the size of the buried blocks are expressed in **Table 1**.

Figure 1a presents the calculated magnetic anomaly for the synthetic model, incorporating 5% random noise. The inversion process converged after 23 iterations in 6.3 s, achieving a normalized misfit of 0.05 (see **Figure 1b**).

Figure 2 displays horizontal and vertical cross-sections of the true and inverted 3D susceptibility models. The horizontal slice is extracted at 75 m depth, while the vertical section is taken along the x-axis at $y = 450$ m. Together, these orthogonal views provide complementary visualization of the subsurface structure. The results demonstrate that the suggested inversion technique effectively reconstructs the synthetic model. In comparison with the true models in panels a and b, the recovered model accurately locates the four blocks in their intended positions, with distinct boundaries. Additionally, the estimated susceptibility values closely align with the actual values of the true blocks.

The model's computed magnetic response is presented in **Figure 3a**. A comparison between this calculated data and the measured data is illustrated in **Figure 3b**. This comparison demonstrates that the calculated data achieves an acceptable match to the observed data, indicating a successful data fitting process.

2.4. Application to the field data

The McFaulds Lake area in Canada is well-known for deposits, rich in nickel, copper, and platinum group elements (Ni-Cu-PGE) such as the Eagle's Nest deposit. This site lies near Webequie, northwestern Ontario. The area is characterized by a highly magnetic ultramafic intrusion of mantle origin, recognized as the 'Ring of Fire'. This intrusion has been emplaced along the edge of a significant granodiorite pluton, within the rock formations of the Sachigo greenstone belt. The area has been the focus of exploration for various economically significant mineral deposits including magmatic deposits of Ni, Cu, and PGE, Chromite mineralization of magmatic origin, Volcanic-hosted massive sulfide deposits as well as Diamond-bearing kimberlite formations (Balch et al. 2010; Lin and Zhdanov, 2018). The Ring of Fire's rocks include mafic metavolcanic flows, felsic metavolcanic flows, pyroclastic rocks and layered mafic to ultramafic intrusions. These intrusions run roughly parallel to the belt's westernmost section, occasionally cutting across it at an angle. They are situated near a large granitoid batholith west of the belt. The main layered intrusion in this area is notable for two types of deposits, at its deeper parts there are high-grade Ni-Cu-PGE deposits and the shallower parts and further east contains stratiform chromite deposits in the intrusion's stratigraphy (Geological Survey and Geological Survey of Canada, 2011).

In the study area, chromite deposits are typically found within layered ultramafic intrusive rocks, often in association with magnetite and serpentine. This association allows for the magnetic tracing of chromite through its potential host rocks. Therefore, airborne geophysical surveys were carried out in the McFaulds Lake area in 2010, gathering magnetic data from the air (Geological Survey and Geological Survey of Canada, 2011). Fig-

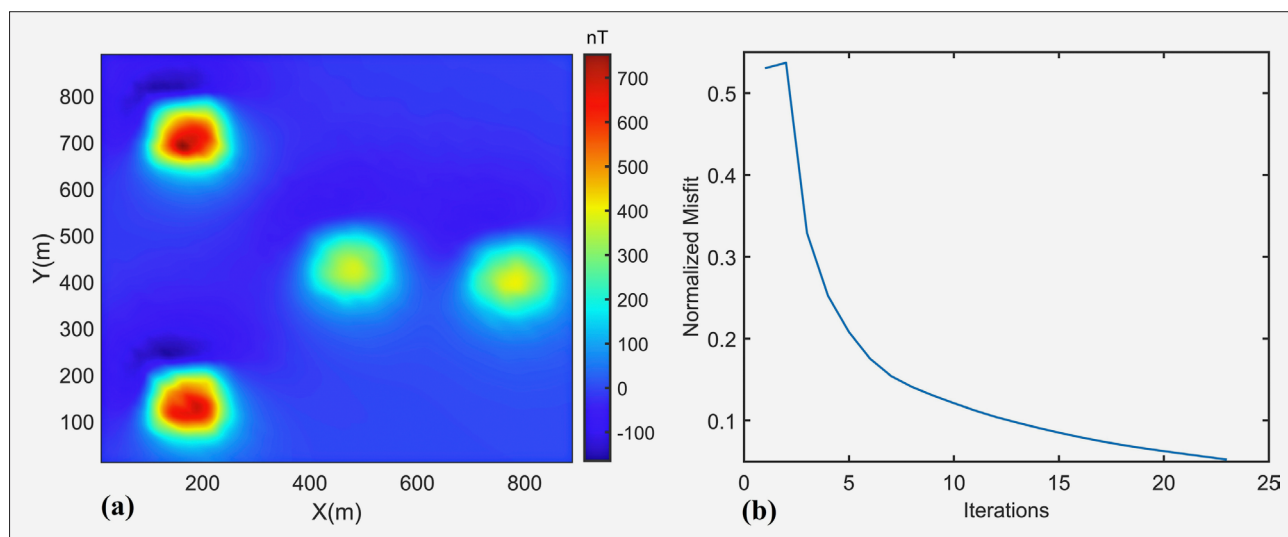


Figure 1. The magnetic anomaly from the synthetic model with 5% Gaussian noise of each datum magnitude (a). The behaviour of the normalized misfit (b).

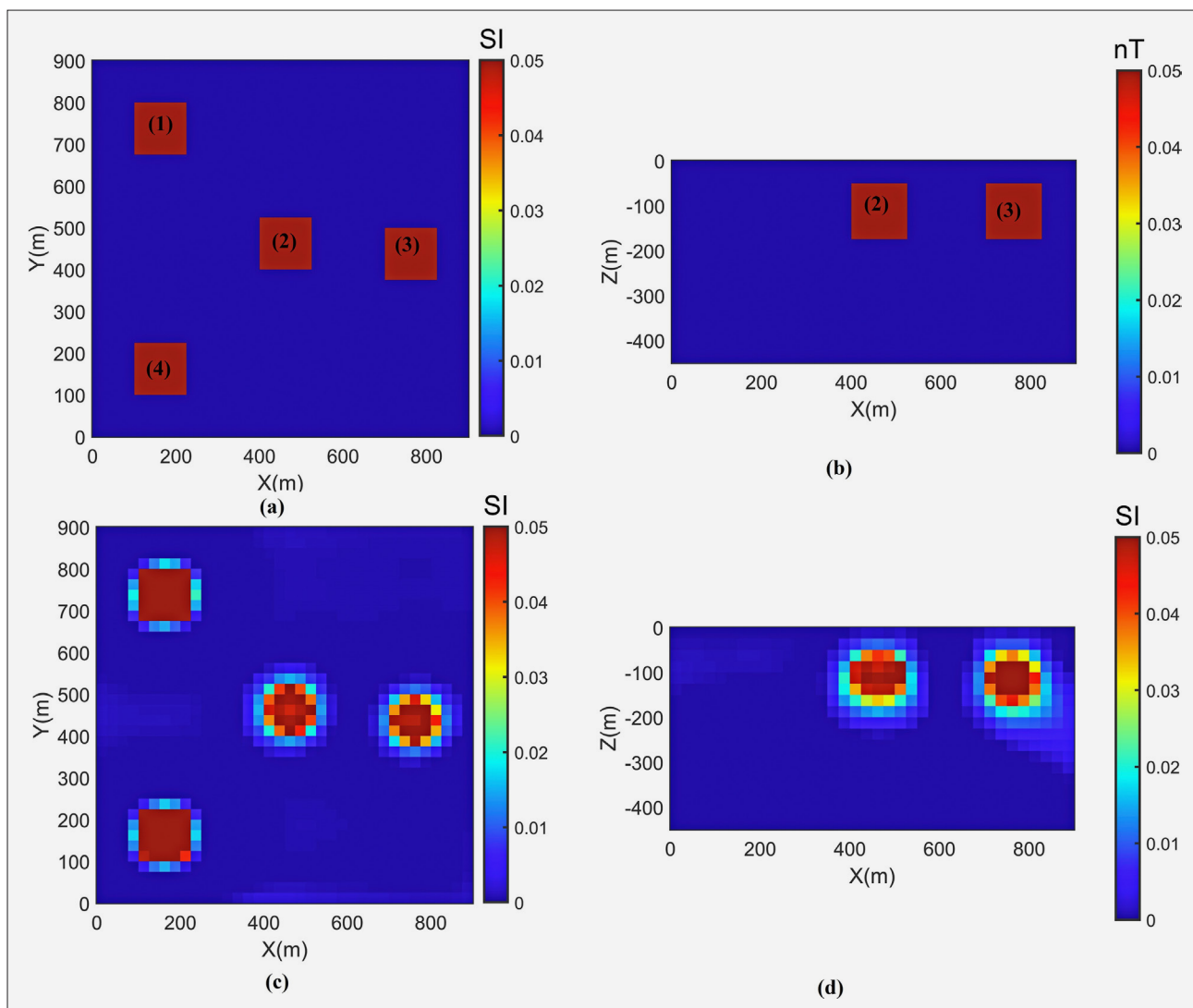


Figure 2. (a) Horizontal plan section of the true susceptibility distribution at a depth of 75 m. (b) A cross-sectional slice of the true susceptibility model at $Y = 450$ m. (c) Plan section through recovered model by inversion. (d) The vertical slice in the inversion result.

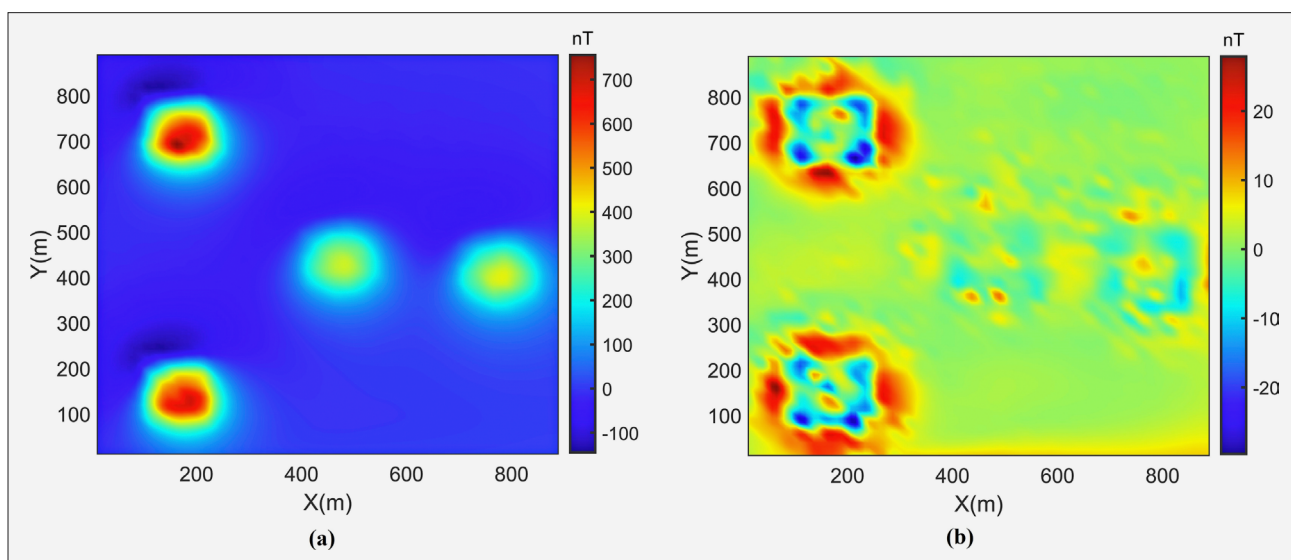


Figure 3. (a) The map of the magnetic anomaly from the focused model. (b) The residual map between computed and original data.

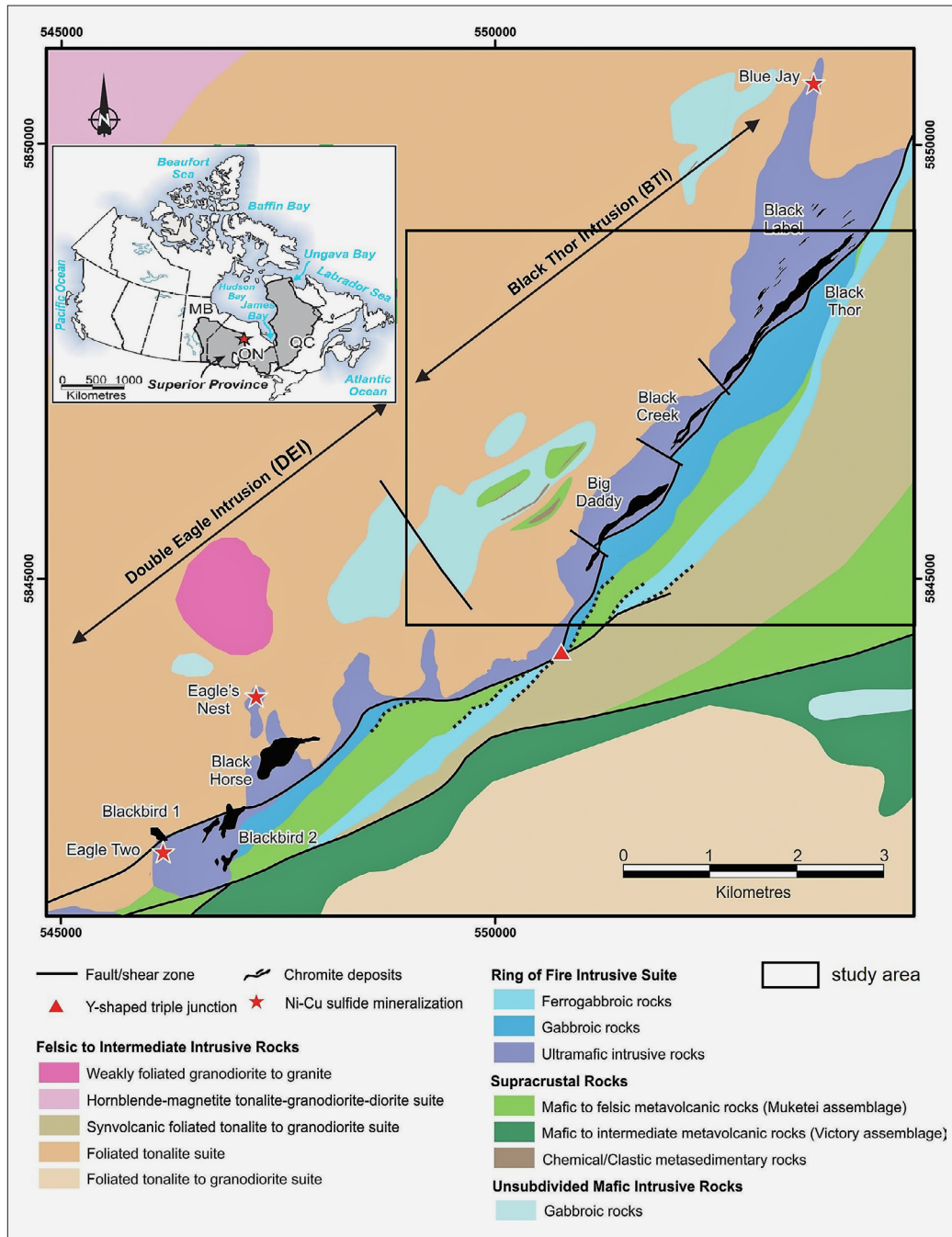


Figure 4. Geological map of the study area (adapted from Laudadio et al. 2022)

Figure 4 displays a geological map of the study area with known mineralizations (Laudadio et al. 2022).

The Ring of Fire intrusive body in the study area contains two main ultramafic intrusions, the Black Thor intrusion (BTI) and the Double Eagle intrusion (DEI), which are associated with significant chromite mineralization. These intrusions host several major deposits, including Black Thor, Black Label, Big Daddy, Black Horse, Blackbird, and Black Creek (see Figure 4). Collectively, the deposits in this region hold an estimated 343 million tonnes of geological resources averaging 32% chromite. Research suggests that the BTI and DEI

were supplied by separate magma conduits. The BTI and DEI intrusions are primarily made up of a thick ultramafic lower section and a thinner mafic upper section. The ultramafic portion consists of dunite, peridotite (mainly harzburgite), pyroxenite, and chromite, all metamorphosed to lower greenschist facies. Within these rocks, dunite and peridotite are largely composed of serpentinized or talc-altered olivine, making up 75–95% of their mineral content. Magnetite is widespread, appearing both as fine disseminated particles and as rims around chromite grains, a result of serpentinization processes. Chromitite mineralization appears in diverse

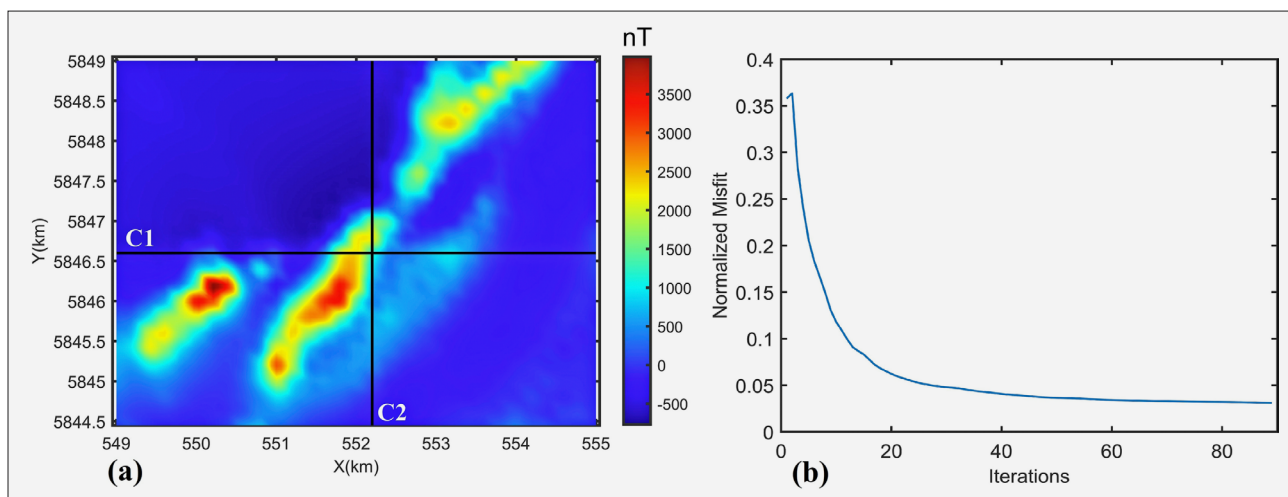


Figure 5. The map of magnetic anomaly over the McFaulds Lake area. The conjunction of the C1 and C2 lines represents the position of the Black Creek deposit (a). The behaviour of the normalized misfit (b).

styles, including finely laminated to thickly bedded layers, variably disseminated grains, and interlayered massive to semi-massive chromite deposits. These occurrences are typically hosted within dunite and peridotite zones. (Laudadio et al. 2022).

To demonstrate how well our proposed method works with field data, we've applied it to a portion of the magnetic data that covers the Black Creek area which is known for its chromite mineralization. **Figure 5a** illustrates the magnetic anomaly of the study area in which the C1 and C2 lines intersect at the location of the Black Creek chromite deposit.

The dimensions of the model domain was set to $6 \text{ km} \times 4.5 \text{ km} \times 2 \text{ km}$ in x, y and z directions and the subsurface region was divided into cube-shaped segments, each measuring 100 m on all sides leading to $60 \times 45 \times 20 = 54000$ cells. We ran the magnetic inversion by the arctangent stabilizing functional and the algorithm has been converged to the solution after 89 iterations in 34.38 s (see **Figure 5b**). **Figure 6** presents a comparison of actual measurements (see **Figure 5a**) and calculated data from the obtained model (see **Figure 6a**) for the total magnetic intensity field. The visual representation demonstrates a high degree of agreement between the observed and predicted data. This close correspondence is further highlighted by the inclusion of a difference map (see **Figure 6b**), which visually depicts the discrepancies between the measured and predicted magnetic field.

Figure 7 illustrates cross-sections in the inverted model of the study area. The panels a and b display vertical slices through the reconstructed magnetic susceptibility distribution along two specific lines, labeled C1 and C2 in **Figure 5a**.

In the C1 cross-section, the inversion results clearly reveal the top boundaries of the identified mineral deposit. However, the deeper portions of this body exhibit lower magnetic properties. Examining the C2 cross-section, the magnetic inversion suggests that the dike structure on the

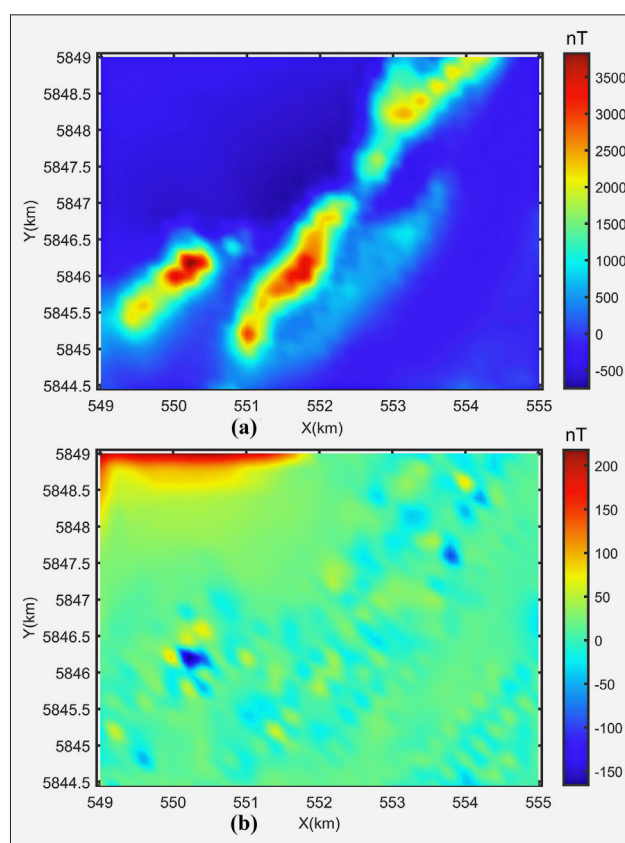


Figure 6. The map of the predicted magnetic data from the model (a). The map of the difference between the observed and predicted data (b).

right side contains a higher concentration of magnetic minerals. This increased magnetism might be indicative of chromite deposits in the Black Creek region.

The panel c presents a horizontal cross-section of anomalous magnetic susceptibility at a depth of 300 m. The horizontal slice, along with the previously mentioned vertical cross-sections, reveals anomalous targets characterized by distinct and partially continuous boundaries.

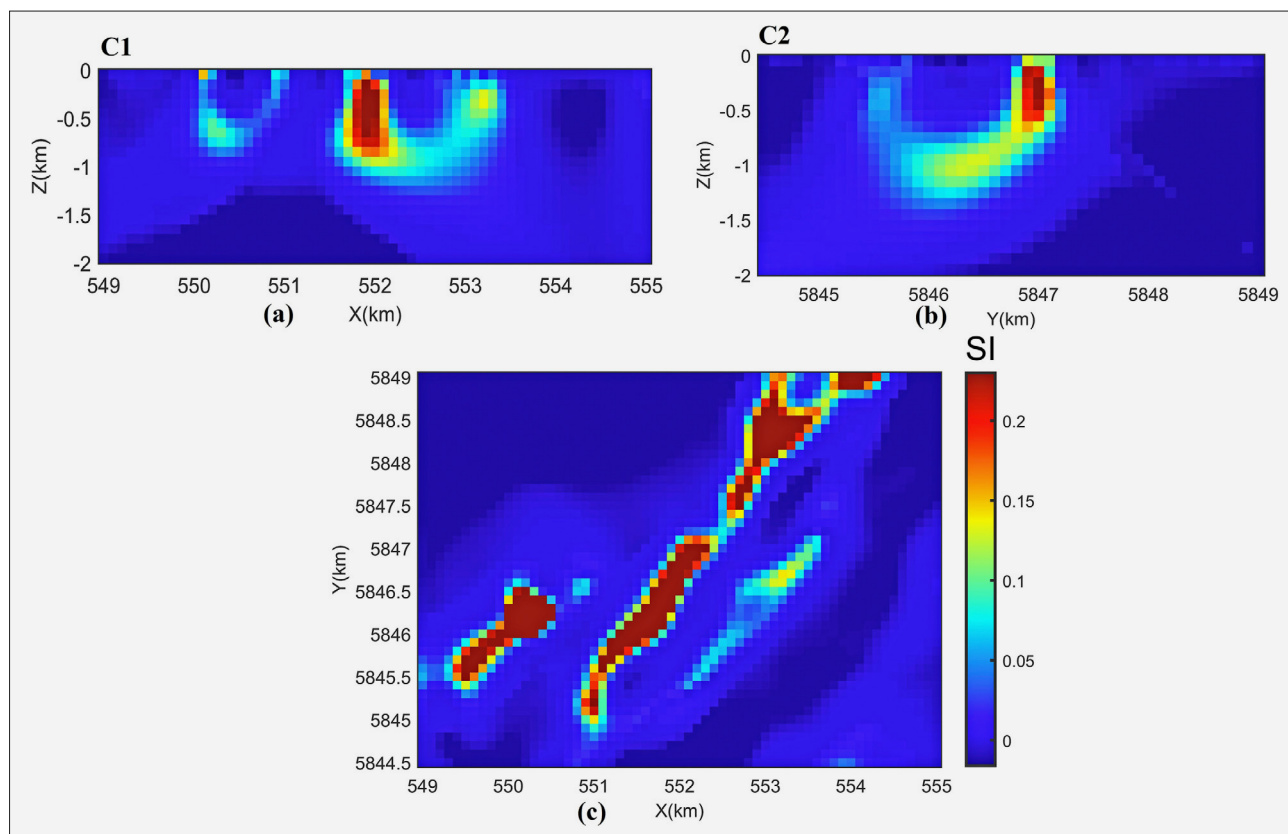


Figure 7. Vertical cross-sections of the recovered anomalous magnetic susceptibility distribution along C1 line (a) and C2 line (b). The horizontal section at the depth of 300 m (c).

This representation offers valuable insight into the nature and distribution of mineral deposits in the area. This approach enhances our understanding of the subsurface geological structures and potential mineral resources. The results agree with those obtained by **Lin and Zhdanov (2018)** using the multinary joint inversion of gravity and magnetic data over the study area.

3. Results and Discussion

The proposed arctangent stabilizer-based inversion method showed excellent performance in both synthetic and field tests. For the synthetic model, the inversion accurately recovered four prismatic blocks with sharp boundaries, achieving convergence after 23 iterations with a normalized misfit of 0.05 despite 5% added noise. Horizontal and vertical cross-sections (see **Figure 2**) showed precise reconstruction of the targets' locations and susceptibilities, while the calculated magnetic response (see **Figure 3a**) closely matched observations, with randomly distributed residuals (see **Figure 3b**) confirming robust data fitting. The method's effectiveness was further validated using aeromagnetic data from Ontario's McFaulds Lake area, where it resolved the Black Creek chromite deposit's structure after 89 iterations. Vertical sections (see **Figures 7a–b**) revealed distinct magnetic anomalies correlating with known miner-

alization, and the 300 m depth slice (see **Figure 7c**) delineated continuous high-susceptibility zones, aligning with prior geological studies. The computation time for synthetic model was 6.3 s and for the real case it was 34.38 s that demonstrate the efficiency of the algorithm.

Key advantages of the arctangent stabilizer include its parameter-free formulation, which eliminates the need for manual focusing parameter tuning, and its ability to recover compact structures without the elongated artifacts seen in exponential stabilizers. The incorporation of depth weighting mitigated magnetic data's inherent depth ambiguity, while RRCG optimization ensured efficient convergence. Though the method assumes dominant induced magnetization, its performance on field data underscores its practicality for mineral exploration. These results advance compact inversion techniques by combining computational efficiency with improved boundary resolution, offering a valuable tool for sharp-boundary target identification in potential-field geophysics.

4. Conclusions

We have developed a method for the inversion of magnetic data that recovers features of the subsurface structure with sharp boundaries. The method employs an arctangent stabilization functional that eliminates the need to determine an optimal focusing parameter, with

other parameters being automatically selected by the algorithm. When applied to magnetic data from a synthetic model, the inversion method produced a satisfactory susceptibility model. The inversion results demonstrated the method's capability to generate compact models that accurately represent the locations and forms of anomalous bodies.

We then applied this method to aeromagnetic data from the McFaulds Lake region, located in northwestern Ontario, Canada. By employing the inversion approach, we were able to generate a plausible geological model. This model proves valuable for guiding exploration efforts aimed at locating magmatic chromite deposits in the study area.

Acknowledgement

The authors gratefully acknowledge the Geological Survey of Canada (GSC) for providing the high-quality aeromagnetic data from the McFaulds Lake area, which were essential for this study. We also extend our appreciation to the scientists and technical staff at the GSC for their efforts in data acquisition, processing, and public dissemination. Their contributions significantly supported the methodological developments and validations presented in this work.

Funding

The authors declare they have received no funds for this paper.

5. References

- Balch, S. J., Mungall, J. E., & Niemi, J. (2010). Present and future geophysical methods for Ni-Cu-PGE exploration: Lessons from McFaulds Lake, northern Ontario. *Society of Economic Geologists Special Publication*, 15, 11–22. <https://doi.org/10.5382/SP.15.2.11>
- Bertete-Aguirre, H., Cherkaev, E., & Oristaglio, M. (2002). Non-smooth gravity problem with total variation penalization functional. *Geophysical Journal International*, 149(2), 499-507. <https://doi.org/10.1046/j.1365-246X.2002.01664.x>
- Bhattacharyya, B. K. (1964). Magnetic anomalies due to prism-shaped bodies with arbitrary polarization. *Geophysics*, 29(4), 517-531. <https://doi.org/10.1190/1.1439386>
- Blakely, R. J. (1996). *Potential theory in gravity and magnetic applications*. Cambridge university press.
- Cuma, M., Wilson, G. A., & Zhdanov, M. S. (2012). Large-scale 3D inversion of potential field data. *Geophysical Prospecting*, 60(6), 1186-1199. <https://doi.org/10.1111/j.1365-2478.2012.01039.x>
- Fedi, M., & Rapolla, A. (1999). 3-D inversion of gravity and magnetic data with depth resolution. *Geophysics*, 64(2), 452-460. <https://doi.org/10.1190/1.1444550>
- Hu, S., Zhao, Y., Qin, T., Rao, C., & An, C. (2017). Traveltime tomography of crosshole ground-penetrating radar based on an arctangent functional with compactness constraints. *Geophysics*, 82(3), H1-H14. <https://doi.org/10.1190/geo2016-0369.1>
- Last, B. J., & Kubik, K. (1983). Compact gravity inversion. *Geophysics*, 48(6), 713-721. <https://doi.org/10.1190/1.1441505>
- Laudadio, A. B., Schetselaar, E. M., Mungall, J. E., & Houlé, M. G. (2022). 3D modeling of the Esker intrusive complex, Ring of Fire intrusive suite, McFaulds Lake greenstone belt, Superior Province: Implications for mineral exploration. *Ore Geology Reviews*, 145, 104886. <https://doi.org/10.1016/j.oregeorev.2022.104886>
- Lelièvre, P. G., Oldenburg, D. W., & Williams, N. C. (2009). Integrating geological and geophysical data through advanced constrained inversions. *Exploration Geophysics*, 40(4), 334-341. <https://doi.org/10.1071/EG09016>
- Li, Y., & Oldenburg, D. W. (1998). 3-D inversion of gravity data. *Geophysics*, 63(1), 109-119. <https://doi.org/10.1190/1.1444302>
- Lin, W., & Zhdanov, M. S. (2018). Joint multinary inversion of gravity and magnetic data using Gramian constraints. *Geophysical Journal International*, 215(3), 1540-1557. <https://doi.org/10.1093/gji/ggy366>
- Marchetti, P., Coraggio, F., Gabbriellini, G., Ialongo, S., & Fedi, M. (2014, October). Large-scale 3D gravity data space inversion in hydrocarbon exploration. In *SEG International Exposition and Annual Meeting* (pp. SEG-2014). SEG.
- Meng, Z. (2018). Three-dimensional potential field data inversion with L0 quasinorm sparse constraints. *Geophysical Prospecting*, 66(3), 626-646. <https://doi.org/10.1111/1365-2478.12593>
- Ontario Geological Survey and Geological Survey of Canada. (2011). Ontario airborne geophysical surveys, gravity gradiometer and magnetic data, grid and profile data (ASCII and Geosoft® formats) and vector data, McFaulds Lake area. Ontario Geological Survey, Geophysical Data Set 1068. <https://www.geologyontario.mndm.gov.on.ca/mndmfiles/pub/data/records/GDS1068.html>
- Peng, G., Liu, Z., Xu, K., Bai, Y., & Du, R. (2018). Efficient 3D inversion of potential field data using fast proximal objective function optimization algorithm. *Journal of Applied Geophysics*, 159, 108-115. <https://doi.org/10.1016/j.jappgeo.2018.07.020>
- Pilkington, M. (2009). 3D magnetic data-space inversion with sparseness constraints. *Geophysics*, 74(1), L7-L15. <https://doi.org/10.1190/1.3043726>
- Portniaguine, O., & Zhdanov, M. S. (1999). Focusing geophysical inversion images. *Geophysics*, 64(3), 874-887. <https://doi.org/10.1190/1.1444596>
- Portniaguine, O., & Zhdanov, M. S. (2002). 3-D magnetic inversion with data compression and image focusing. *Geophysics*, 67(5), 1532-1541. <https://doi.org/10.1190/1.1512749>
- Rao, D. B., & Babu, N. R. (1991). A rapid method for three-dimensional modeling of magnetic anomalies. *Geophysics*, 56(11), 1729-1737. <https://doi.org/10.1190/1.1442985>
- Rezaie, M. (2019). 3D non-smooth inversion of gravity data by zero order minimum entropy stabilizing functional.

- Physics of the Earth and Planetary Interiors*, 294, 106275. <https://doi.org/10.1016/j.pepi.2019.106275>
- Rezaie, M. (2020). A sigmoid stabilizing function for fast sparse 3D inversion of magnetic data. *Near Surface Geophysics*, 18(2), 149-159. <https://doi.org/10.1002/nsg.12091>
- Rezaie, M. (2023). Focusing inversion of gravity data with an error function stabilizer. *Journal of Applied Geophysics*, 208, 104890. <https://doi.org/10.1016/j.jappgeo.2022.104890>
- Rezaie, M., Moradzadeh, A., & Nejati Kalate, A. (2017). 3D gravity data-space inversion with sparseness and bound constraints. *Journal of Mining and Environment*, 8(2), 227-235. <https://doi.org/10.22044/jme.2017.4976.1363>
- Tikhonov, A.N., Arsenin, V.Y., 1977. *Solution of Ill-Problems*. Winston and Sons, Washington.
- Xiang, Y., Yu, P., Zhang, L., Feng, S., & Utada, H. (2017). Regularized magnetotelluric inversion based on a minimum support gradient stabilizing functional. *Earth, planets and space*, 69, 1-18. <https://doi.org/10.1186/s40623-017-0651-1>
- Zhao, C., Yu, P., & Zhang, L. (2016). A new stabilizing functional to enhance the sharp boundary in potential field regularized inversion. *Journal of Applied Geophysics*, 135, 356-366. <https://doi.org/10.1016/j.jappgeo.2016.10.024>
- Zhdanov, M. S. (2015). *Inverse theory and applications in geophysics*. Elsevir. <https://doi.org/10.1016/C2012-0-03334-0>

SAŽETAK

Magnetska inverzija za pronalaženje kompaktnih struktura pomoću arkus tangens stabilizatora

Ova studija predstavlja novu metodu za inverziju magnetskih podataka koristeći se tehnikom fokusirajuće inverzije. Metoda primjenjuje stabilizirajući funkcional arkus tangensa, koji se reformulira u pseudokvadratni oblik pomoću matrice težina. Za optimizaciju procesa korištena je metoda ponovno ponderiranoga regulariziranog konjugiranog gradijenta (RRCG). Predložena tehnika učinkovita je u obnavljanju kompaktnih struktura u podzemnim strukturama bez potrebe za fokusirajućim parametrom. Metoda inverzije uključuje konstruiranje funkcije cilja za minimizaciju, koja obuhvaća razliku između promatranih i predviđenih podataka i odstupanje modela od očekivanih karakteristika, što je poznato kao stabilizirajući funkcional. Komponenta prilagodbe podataka određuje koliko se rezultati inverzije podudaraju s promatranim mjerenjima, dok termin regularizacije modela utječe na specifična željena svojstva rekonstruirane distribucije gustoće. Studija pokazuje učinkovitost predložene tehnike primjenom na sintetički skup podataka i jedan stvarni aeromagnetski skup podataka iz područja jezera McFaulds u Ontariju, Kanada.

Ključne riječi:

magnetski, inverzija, stabilizator, arkus tangens, jezero McFaulds

Author's contribution

Sahar Moazam (Dr): conceptualization, investigation and software. **Mohammad Rezaie** (Dr): conceptualization, preparing the main codes and writing.

All authors have read and agreed to the published version of the manuscript.